

# A Coupled Conforming–Nonconforming Galerkin Method for Poisson’s Equation on Curved Domains

Qingguang Guan <sup>\*</sup> <sup>1</sup> and Wenju Zhao <sup>†</sup> <sup>2</sup>

<sup>1</sup>School of Mathematics and Natural Sciences, University of Southern Mississippi,  
Hattiesburg, MS 39406, USA

<sup>2</sup>School of Mathematics, Shandong University, Jinan, Shandong 250100, China

## Abstract

A coupled conforming–nonconforming Galerkin method is proposed for Poisson’s equation on two-dimensional curved domains. The method applies a weak Galerkin discretization only on a thin boundary layer of curvilinear elements near the curved boundary, while using a standard continuous Galerkin discretization in the polygonal interior. In this way, geometric flexibility is retained where it is needed most, and the number of nonconforming degrees of freedom is significantly reduced. A key ingredient is a mixed interpolation–projection operator on curvilinear weak Galerkin elements, combining  $L^2$  edge projections with conforming nodal interpolation on the interface side to ensure compatibility with the continuous Galerkin trace. Based on this construction, we prove an optimal a priori error estimate of order  $O(h^k)$  in the energy norm under the basic geometric assumptions of the method, and an optimal  $L^2(\Omega)$  estimate of order  $O(h^{k+1})$  under the additional elliptic dual regularity assumption. Numerical experiments confirm the theoretical rates and demonstrate substantial savings in degrees of freedom compared with a fully weak Galerkin discretization.

**Keywords:** Weak Galerkin method; continuous Galerkin method; curved domains; curvilinear elements; conforming–nonconforming coupling; a priori error estimates.

**MSC2020:** 65N30, 65N12, 35J25.

## 1 Introduction

Accurate numerical simulation of partial differential equations on *curved domains* requires controlling two coupled error mechanisms: the approximation of the solution space and the approximation of the geometry. Even for the Poisson problem

$$-\Delta u = f \quad \text{in } \Omega, \quad u = 0 \quad \text{on } \partial\Omega,$$

a naive polygonal approximation of a smooth boundary can degrade convergence, especially for higher-order methods, unless geometry errors are treated carefully.

<sup>\*</sup>First author. Email: qingguang.guan@usm.edu

<sup>†</sup>Corresponding author. Email: zhaowj@sdu.edu.cn. Wenju Zhao was partially supported by National Key R& D Program of China (No. 2023YFA10089033), Natural Science Foundation of Shandong Province (No. ZR2023ZD38), National Natural Science Foundation of China (No.12131014).

Submitted to *Numerical Methods for Partial Differential Equations*: March 8, 2026. Accepted: June 18, 2026.

A classical remedy is to employ *boundary-fitted curved elements*, such as isoparametric finite elements. However, maintaining the optimal convergence rate of these methods is contingent upon the strict invertibility of the Jacobian matrix associated with the diffeomorphic mapping from the reference element to the physical element. Furthermore, optimal error bounds require bounds on the higher-order derivatives of this mapping, which inherently rely on sufficient smoothness of the curved boundary. Constructing such valid mappings is a highly non-trivial task, see [18, 27, 8]. An alternative is to decouple the mesh from the boundary through *unfitted/embedded* techniques, including fictitious domain, immersed/cut finite element methods, which enforce boundary conditions weakly and add stabilization on cut elements, see [21, 16, 5]. Such methods avoid curved meshes and are good at dealing with moving interfaces/boundaries, but they are considerably more difficult to implement and use robustly in 3D than in 2D. In 3D a cut cell becomes an arbitrary polyhedron (possibly with dozens of faces). Accurate volume integration over these shapes requires sophisticated algorithms. A third successful direction is the development of *polygonal* discretizations that naturally accommodate complex boundaries and interfaces, such as discontinuous Galerkin (DG) [6, 7, 1, 3, 2], hybridizable-DG (HDG) [9, 22, 15, 17], virtual element methods (VEM) [24, 23, 10], weak Galerkin (WG) methods [12, 13, 25, 19] and many others.

Nonconforming methods have proved particularly attractive for complex geometries because their degrees of freedom are naturally associated with element boundaries and can be adapted to curved edges/faces. For instance, in the WG framework, recent work [14] has introduced high-order WG formulations on *curvilinear polytopal* meshes with Lipschitz continuous curved edges/faces, enabling convergence rates that are independent of the geometry approximation under suitable regularity assumptions.

While DG/HDG/nonconforming-VEM/WG methods offer strong geometric flexibility, they also introduce extra interface unknowns (traces, numerical fluxes, or boundary variables) throughout the domain. In many applications, however, the *primary difficulty is the curved boundary*, whereas the interior of the domain is geometrically simple and does not benefit from a fully nonconforming treatment. This observation motivates a *coupled* conforming–nonconforming strategy: use a geometry-robust nonconforming method only in a thin layer adjacent to  $\partial\Omega$ , and retain a standard conforming method in the interior. Due to its simplicity and flexibility, which facilitates analysis, we select the Weak Galerkin method as the nonconforming component and the Continuous Galerkin (CG) method as the conforming component to develop a coupled conforming–nonconforming Galerkin method. Other nonconforming methods remain valid candidates. This philosophy is consistent with a long line of *hybrid couplings* in the Galerkin literature. Coupled continuous/discontinuous Galerkin schemes were introduced to deploy discontinuous formulations only where additional flexibility is required (e.g., nonsmooth solution features), while preserving the efficiency of continuous elements elsewhere, see [11]. In the WG setting, coupled WG–CG formulations have been studied for *physical* interface problems, see [20] for Stokes–Darcy, where different discretizations are naturally used in different subregions and are coupled across an interface. The present work differs in that the interface is not fixed; rather, it separates a curved boundary layer—which thins as the mesh is refined—from a polygonal interior. Additionally, our method solves a single-valued PDE on a single domain, necessitating fundamentally different techniques and error analysis.

We propose and analyze a coupled conforming–nonconforming Galerkin method for Poisson’s equation on two-dimensional  $C^{0,1}$  domains (Lipschitz-continuous boundary). The method employs:

- a **boundary-layer weak Galerkin discretization** on curvilinear elements whose outer side lies on  $\partial\Omega$ , designed to treat curved boundaries directly;

- a **standard continuous Galerkin discretization** on a triangulation of the polygonal interior, reducing degrees of freedom significantly;
- a **strong coupling** across the artificial interface  $\Gamma$  between the two regions, so that the global trial space remains conforming across  $\Gamma$  while allowing nonconforming traces on the outer and outer–inner sides of boundary-layer elements;
- a new **mixed interpolation–projection operator** on curvilinear WG elements, using  $L^2$  edge projections on the curved/outer sides and conforming nodal interpolation on the inner side to match the CG trace on  $\Gamma$ .

On shape-regular curvilinear elements (star-shaped with a uniform chunkiness parameter), we establish stability and approximation estimates for the mixed interpolation–projection operator, and derive optimal order error estimates:  $\mathcal{O}(h^k)$  in the natural energy norm under the geometric assumptions stated below, and  $\mathcal{O}(h^{k+1})$  in  $L^2(\Omega)$  under the additional dual elliptic regularity assumption introduced in Section 4.3. From a practical standpoint, the coupled scheme reduces the global number of degrees of freedom compared to a nonconforming discretization while preserving optimal convergence rate, since the nonconforming unknowns are restricted to the boundary layer.

The paper is organized as follows. Section 2 collects geometric assumptions and auxiliary approximation tools on curvilinear elements and introduces the interpolation–projection operator. Section 3 presents the coupled WG–CG scheme and proves well-posedness. Section 4 establishes energy and  $L^2$  error estimates. Section 5 reports numerical experiments on the unit disk that confirm the theoretical convergence rates and illustrate the reduction in degrees of freedom.

## 2 Preliminaries and Auxiliary Lemmas

While this paper focuses exclusively on two-dimensional domains with curved boundaries, the analysis and methodology can be readily extended to three dimensions. In this section, we collect the necessary geometric definitions, trace inequalities, and polynomial approximation results required to analyze the interpolation-projection weak Galerkin operator on curvilinear elements.

### 2.1 Domain Properties and Shape Regularity

Let  $\Omega \subset \mathbb{R}^2$  be a bounded domain with a  $C^{0,1}$  curved boundary. This Lipschitz regularity is the basic geometric assumption used to define the boundary layer and invoke the local trace and approximation results on curvilinear elements. The mesh is constructed in two steps: (1) create a “boundary layer,” as shown in the left panel of Figure 1; every element in this layer can be represented by the enlarged element as in the right panel; (2) after the boundary layer is created, the remaining interior region is a polygon, which is then triangulated.

Let  $D$  denote a curvilinear element in the boundary layer, whose curved side is a subset of  $\partial\Omega$ . This element  $D$  has four sides: one outer side, two outer–inner sides, and one inner side. On  $D$ , we use the  $L^2$  projection from  $L^2(e)$  onto  $\mathbb{P}_k|_e$  (the trace sense as in [14]) when  $e$  is an outer side or an outer–inner side, and we use the conforming interpolation onto  $\mathbb{P}_k(e)$  when  $e$  is the inner side. Let  $T$  denote a triangular element in the interior. With this design, we apply the weak Galerkin method only in the boundary layer and the CG method in the interior. This hybrid approach combines the advantages of both methods: it provides a better treatment of the curved boundary while reducing the number of unknowns in the interior region.

Following Guan, et al.[14], we require the element  $D$  to satisfy the following shape-regularity assumptions:

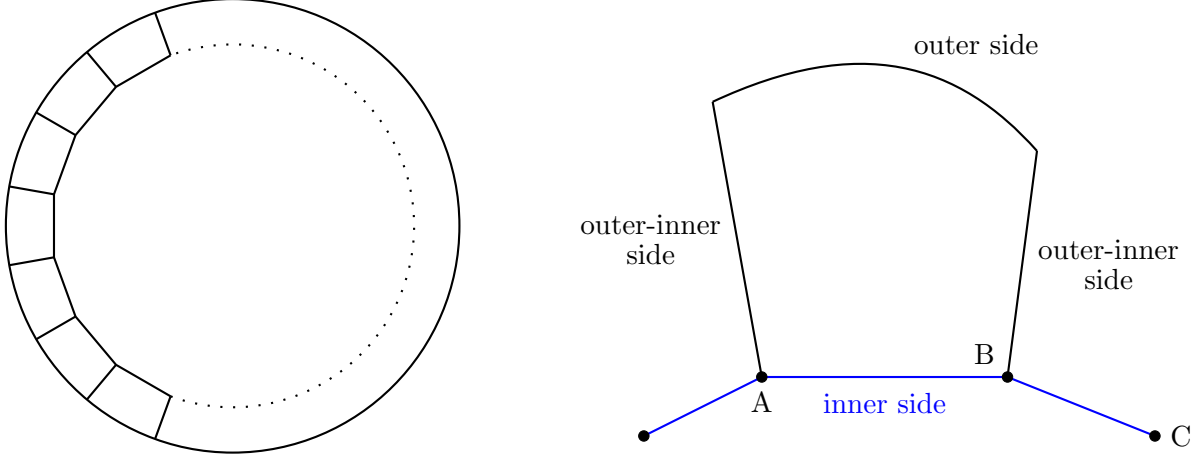


Figure 1: **Left:** the “boundary layer” of the mesh for a two-dimensional domain  $\Omega$ . **Right:** an enlarged element from the boundary layer, it doesn't need to be convex. At point  $B$ , there is only one unknown. The numerical solution  $u_h$  on the interface  $\overline{AB}-\overline{BC}$  is continuous at point  $B$ , but  $u_h$  on the outer-inner side is not continuous at  $B$ . Continuity of  $u_h$  follows the same pattern at other end points of the inner sides.

**Assumption 1** (Shape Regularity [14]). *The element  $D$  is shape-regular if it satisfies:*

- (A1)  $D$  is a curvilinear polygon with a  $C^{0,1}$  curved side and diameter  $h_D$ .
- (A2)  $D$  is star-shaped with respect to a disc  $\mathfrak{B}_D \subset D$  with radius  $\rho_D h_D$ , where  $0 < \rho_D < 1/2$ ; here  $\rho_D$  is the dimensionless relative radius parameter.
- (A3) The parameter  $\rho_D$  has a uniform lower bound  $0 < \rho_{\min} < \rho_D$ .

Assumption (A2) is particularly crucial as it mathematically permits the application of the Averaged Taylor Polynomial theory over the curved element  $D$ . Let  $A \lesssim B$  denote  $A \leq (\text{constant})B$ .

## 2.2 The Weak Galerkin and the Interpolation-Projection Operator

Let  $V(D)$  be the space of discontinuous functions defined on  $D$  and its boundary  $\partial D$ :

$$V(D) = \{v = (v_0, v_b) : v_0 \in L^2(D), v_b \in L^2(\partial D)\}. \quad (1)$$

For any  $v \in V(D)$ , the weak gradient  $\nabla_w v \in [\mathbb{P}_{k-1}(D)]^2$  is defined as the unique polynomial satisfying:

$$(\nabla_w v, \vec{q})_D := -(v_0, \nabla \cdot \vec{q})_D + \langle v_b, \vec{q} \cdot \vec{n} \rangle_{\partial D}, \quad \forall \vec{q} \in [\mathbb{P}_{k-1}(D)]^2. \quad (2)$$

In our scheme, the boundary  $\partial D$  is partitioned into two disjoint sets:  $\partial D_{proj}$  (the outer and outer-inner sides) and  $\partial D_{int}$  (the inner side). We define the interpolation-projection operator  $Q_h \xi|_D = (Q_{k,D}^0 \xi, Q_{b,D}^\partial \xi)$  for  $\xi \in H^{k+1}(D)$  as follows:

**Definition 1** (Interpolation-Projection Operator  $Q_h$ ). *Let  $\partial D_{proj}$  denote the union of the outer-side and outer-inner sides of  $D$ , and  $\partial D_{int}$  denote the inner-side of  $D$ . We define the projection*

operator  $Q_h \xi|_D = (Q_{k,D}^0 \xi, Q_{b,D}^\partial \xi)$ , where  $Q_{k,D}^0$  is the  $L^2$  projection from  $L^2(D)$  to  $\mathbb{P}_k(D)$ , and on each side  $e \subset \partial D$ :

$$Q_{b,D}^\partial \xi|_e = \begin{cases} Q_{k,e}^\partial \xi, & \text{if } e \in \partial D_{proj} \text{ (} L^2 \text{ projection to } \mathbb{P}_k|_e \text{),} \\ I_{k,e}^\partial \xi, & \text{if } e \in \partial D_{int} \text{ (conforming nodal interpolation to } \mathbb{P}_k(e) \text{).} \end{cases} \quad (3)$$

Throughout the paper, boundary traces are understood on the closure  $\overline{D}$ . In particular, if  $w$  is continuous on  $\overline{D}$ , then  $\|w\|_{L^\infty(\overline{D})} = \|w\|_{L^\infty(D)}$ . Thus, for functions continuous on  $\overline{D}$ , the norms  $\|\cdot\|_{L^\infty(D)}$  and  $\|\cdot\|_{L^\infty(\overline{D})}$  are used interchangeably.

To bound boundary terms by volume terms, we rely on the following standard inequalities established for shape-regular curvilinear elements.

**Lemma 1** (Trace Inequality [14, Lemma 2.2]). *If  $D$  is shape-regular, then for any side  $e \subset \partial D$  and any  $v \in H^1(D)$ :*

$$\|v\|_{L^2(e)}^2 \lesssim h_D^{-1} \|v\|_{L^2(D)}^2 + h_D \|\nabla v\|_{L^2(D)}^2. \quad (4)$$

**Lemma 2** (Discrete Inverse Trace Inequality [14, Lemma 2.4]). *If  $D$  is shape-regular, then for any polynomial vector field  $\vec{q} \in [\mathbb{P}_k(D)]^2$ :*

$$\|\vec{q}\|_{L^2(\partial D)} \lesssim h_D^{-1/2} \|\vec{q}\|_{L^2(D)}. \quad (5)$$

To properly bound the approximation error over both  $L^2$  projections and nodal interpolations simultaneously, we utilize the Averaged Taylor Polynomial (see Definition 4.1.3 in [4]).

**Lemma 3** (Averaged Taylor Polynomial Bounds [4]). *Suppose  $D \subset \mathbb{R}^2$  is star-shaped with respect to a disc (satisfying Assumption 1). Let  $k \geq 1$ . For any  $\xi \in H^{k+1}(D)$ , there exists a polynomial  $p \in \mathbb{P}_k(D)$  (the Averaged Taylor Polynomial of degree  $k$ ) such that the following approximation bounds hold simultaneously:*

$$\|\xi - p\|_{L^2(D)} \lesssim h_D^{k+1} |\xi|_{H^{k+1}(D)}, \quad (6)$$

$$\|\nabla(\xi - p)\|_{L^2(D)} \lesssim h_D^k |\xi|_{H^{k+1}(D)}, \quad (7)$$

$$\|\xi - p\|_{L^\infty(D)} \lesssim h_D^k |\xi|_{H^{k+1}(D)}. \quad (8)$$

*Proof.* The polynomial  $p$  is defined as the Averaged Taylor Polynomial (Definition 4.1.3 in [4]). The  $L^2(D)$  and  $H^1(D)$  volume bounds (6) and (7) follow directly from the Bramble-Hilbert Lemma (Lemma 4.3.8 in [4]) evaluated at  $m = k + 1$  and  $p = 2$ . The  $L^\infty(D)$  bound (8) follows from Proposition 4.3.2 in [4] (utilizing the Sobolev embedding  $H^{k+1}(D) \hookrightarrow L^\infty(D)$  since  $k + 1 - 2/2 = k \geq 1$ ).  $\square$

The stability property of the 1D nodal interpolation used on the inner side  $e \in \partial D_{int}$  is shown in the following Lemma.

**Lemma 4** (1D Nodal Interpolant Stability). *Let  $I_{k,e}^\partial : C^0(e) \rightarrow \mathbb{P}_k(e)$  be the standard nodal interpolation of degree  $k$  on a 1D edge  $e$ . For any continuous function  $v \in C^0(e)$ , we have the  $L^\infty$  stability bound:*

$$\|I_{k,e}^\partial v\|_{L^\infty(e)} \leq \Lambda_k \|v\|_{L^\infty(e)}, \quad (9)$$

where  $\Lambda_k$  is the Lebesgue constant for the chosen nodal distribution on  $\mathbb{P}_k(e)$ . Furthermore,  $I_{k,e}^\partial p = p$  for any polynomial  $p \in \mathbb{P}_k(e)$ .

**Lemma 5** (Estimation of the Interpolation-Projection Operator). *Let  $Q_h$  be the operator defined above. Assuming  $D$  is shape-regular and  $k \geq 1$ , for any  $\xi \in H^{k+1}(D)$ , we have*

$$(\nabla_w Q_h \xi, \vec{q})_D = (\mathbb{Q}_{k-1,D} \nabla \xi, \vec{q})_D + \langle Q_{b,D}^\partial \xi - \xi, \vec{q} \cdot \vec{n} \rangle_{\partial D}, \quad \forall \vec{q} \in [\mathbb{P}_{k-1}(D)]^2, \quad (10)$$

$$|\langle Q_{b,D}^\partial \xi - \xi, \vec{q} \cdot \vec{n} \rangle_{\partial D}| \lesssim h_D^k \|\xi\|_{H^{k+1}(D)} \|\vec{q}\|_{L^2(D)}, \quad (11)$$

$$\|\nabla_w Q_h \xi - \mathbb{Q}_{k-1,D} \nabla \xi\|_{L^2(D)} \lesssim h_D^k \|\xi\|_{H^{k+1}(D)}, \quad (12)$$

where  $\nabla_w$  is the weak gradient operator,  $\mathbb{Q}_{k-1,D}$  is the  $L^2$  projection onto  $[\mathbb{P}_{k-1}(D)]^2$ , and the hidden constants depend only on the shape regularity parameters and polynomial degree  $k$ .

*Proof. Part 1: Prove (10).* Using the definition of the weak gradient (2), applying integration by parts, and utilizing the properties of the  $L^2$  projections  $\mathbb{Q}_{k-1,D}$  and  $Q_{k,D}^0$ , we have:

$$\begin{aligned} (\nabla_w Q_h \xi, \vec{q})_D &= -(Q_{k,D}^0 \xi, \nabla \cdot \vec{q})_D + \langle Q_{b,D}^\partial \xi, \vec{q} \cdot \vec{n} \rangle_{\partial D} \\ &= -(\xi, \nabla \cdot \vec{q})_D + \langle \xi, \vec{q} \cdot \vec{n} \rangle_{\partial D} + \langle Q_{b,D}^\partial \xi - \xi, \vec{q} \cdot \vec{n} \rangle_{\partial D} \\ &= (\nabla \xi, \vec{q})_D + \langle Q_{b,D}^\partial \xi - \xi, \vec{q} \cdot \vec{n} \rangle_{\partial D} \\ &= (\mathbb{Q}_{k-1,D} \nabla \xi, \vec{q})_D + \langle Q_{b,D}^\partial \xi - \xi, \vec{q} \cdot \vec{n} \rangle_{\partial D}. \end{aligned}$$

**Part 2: Averaged Taylor Polynomial Estimates.** To prove (11), we first apply the Cauchy-Schwarz inequality and the discrete inverse trace inequality for polynomials (Lemma 2), which implies  $\|\vec{q}\|_{L^2(\partial D)} \lesssim h_D^{-1/2} \|\vec{q}\|_{L^2(D)}$ :

$$\begin{aligned} |\langle Q_{b,D}^\partial \xi - \xi, \vec{q} \cdot \vec{n} \rangle_{\partial D}| &\leq \sum_{e \subset \partial D} \|Q_{b,D}^\partial \xi - \xi\|_{L^2(e)} \|\vec{q} \cdot \vec{n}\|_{L^2(e)} \\ &\lesssim h_D^{-1/2} \|\vec{q}\|_{L^2(D)} \sum_{e \subset \partial D} \|Q_{b,D}^\partial \xi - \xi\|_{L^2(e)}. \end{aligned} \quad (13)$$

We must bound the boundary error  $\|Q_{b,D}^\partial \xi - \xi\|_{L^2(e)}$ . Let  $p \in \mathbb{P}_k(D)$  be the **Averaged Taylor Polynomial** of degree  $k$  of  $\xi$  over  $D$ . Because  $D$  satisfies the shape regularity conditions (Assumption 1), Lemma 3 guarantees that this single polynomial  $p$  satisfies optimal bounds simultaneously in multiple norms.

Specifically, Lemma 3 provides the  $L^\infty(D)$  volume bound:

$$\|\xi - p\|_{L^\infty(D)} \lesssim h_D^k |\xi|_{H^{k+1}(D)} \leq h_D^k \|\xi\|_{H^{k+1}(D)}, \quad (14)$$

as well as the standard  $L^2(D)$  and  $H^1(D)$  volume estimates:

$$\|\xi - p\|_{L^2(D)} \lesssim h_D^{k+1} \|\xi\|_{H^{k+1}(D)} \quad \text{and} \quad \|\nabla(\xi - p)\|_{L^2(D)} \lesssim h_D^k \|\xi\|_{H^{k+1}(D)}. \quad (15)$$

Substituting these into the continuous trace inequality (Lemma 1) applied to the error  $v = \xi - p$ , we obtain the  $L^2(e)$  boundary trace bound:

$$\begin{aligned} \|\xi - p\|_{L^2(e)}^2 &\lesssim h_D^{-1} \|\xi - p\|_{L^2(D)}^2 + h_D \|\nabla(\xi - p)\|_{L^2(D)}^2 \\ &\lesssim h_D^{-1} \left( h_D^{k+1} \|\xi\|_{H^{k+1}(D)} \right)^2 + h_D \left( h_D^k \|\xi\|_{H^{k+1}(D)} \right)^2 \\ &\lesssim h_D^{2k+1} \|\xi\|_{H^{k+1}(D)}^2, \end{aligned} \quad (16)$$

which yields:

$$\|\xi - p\|_{L^2(e)} \lesssim h_D^{k+1/2} \|\xi\|_{H^{k+1}(D)}. \quad (17)$$

**Part 3: Boundary Error Bounds.** We split the sum over the boundary edges into two cases, utilizing the same polynomial  $p$  for both to apply the triangle inequality.

*Case 1: Outer and outer-inner sides ( $e \in \partial D_{proj}$ ).*

Here,  $Q_{b,D}^\partial$  is the  $L^2(e)$  projection, which preserves polynomials of degree  $k$  (i.e.,  $Q_{b,D}^\partial p = p$ ). By the  $L^2$  projection's best-approximation property and (17):

$$\|Q_{b,D}^\partial \xi - \xi\|_{L^2(e)} \leq \|\xi - p\|_{L^2(e)} \lesssim h_D^{k+1/2} \|\xi\|_{H^{k+1}(D)}. \quad (18)$$

*Case 2: Inner side ( $e \in \partial D_{int}$ ).*

Here,  $Q_{b,D}^\partial$  is the conforming nodal interpolation operator  $I_{k,e}^\partial$ , which also preserves polynomials of degree  $k$  (i.e.,  $I_{k,e}^\partial p = p$  by Lemma 4). By the triangle inequality:

$$\|I_{k,e}^\partial \xi - \xi\|_{L^2(e)} \leq \|\xi - p\|_{L^2(e)} + \|I_{k,e}^\partial(\xi - p)\|_{L^2(e)}. \quad (19)$$

The first term is bounded by  $h_D^{k+1/2} \|\xi\|_{H^{k+1}(D)}$  via (17). For the second term, we use the  $L^\infty(e)$  stability of the 1D nodal interpolation (Lemma 4), followed by the volume bound (14):

$$\begin{aligned} \|I_{k,e}^\partial(\xi - p)\|_{L^2(e)} &\lesssim h_e^{1/2} \|I_{k,e}^\partial(\xi - p)\|_{L^\infty(e)} \\ &\lesssim h_D^{1/2} \|\xi - p\|_{L^\infty(e)} \\ &\leq h_D^{1/2} \|\xi - p\|_{L^\infty(D)} \\ &\lesssim h_D^{1/2} \left( h_D^k \|\xi\|_{H^{k+1}(D)} \right) = h_D^{k+1/2} \|\xi\|_{H^{k+1}(D)}. \end{aligned} \quad (20)$$

Summing these bounds gives  $\|I_{k,e}^\partial \xi - \xi\|_{L^2(e)} \lesssim h_D^{k+1/2} \|\xi\|_{H^{k+1}(D)}$ .

**Part 4: Conclusion of the Proof.** Combining the estimates from Case 1 and Case 2 back into (13), we obtain:

$$|\langle Q_{b,D}^\partial \xi - \xi, \vec{q} \cdot \vec{n} \rangle_{\partial D}| \lesssim h_D^{-1/2} \|\vec{q}\|_{L^2(D)} \left( h_D^{k+1/2} \|\xi\|_{H^{k+1}(D)} \right) = h_D^k \|\xi\|_{H^{k+1}(D)} \|\vec{q}\|_{L^2(D)}, \quad (21)$$

which proves (11).

Finally, to prove (12), let  $\vec{q} = \nabla_w Q_h \xi - \mathbb{Q}_{k-1,D} \nabla \xi \in [\mathbb{P}_{k-1}(D)]^2$ . Rearranging (10), we get:

$$\|\vec{q}\|_{L^2(D)}^2 = (\vec{q}, \vec{q})_D = \langle Q_{b,D}^\partial \xi - \xi, \vec{q} \cdot \vec{n} \rangle_{\partial D}. \quad (22)$$

Applying the newly established bound (11), we have:

$$\|\vec{q}\|_{L^2(D)}^2 \lesssim h_D^k \|\xi\|_{H^{k+1}(D)} \|\vec{q}\|_{L^2(D)}. \quad (23)$$

If  $\|\vec{q}\|_{L^2(D)} = 0$ , then (12) is immediate. Otherwise, dividing both sides by  $\|\vec{q}\|_{L^2(D)}$  yields (12) and completes the proof.  $\square$

## 3 The Coupled WG-CG Method

### 3.1 Domain Partition and Function Spaces

Let  $\Omega \subset \mathbb{R}^2$  be a bounded domain with a curved boundary  $\partial\Omega$ . The domain is partitioned into two disjoint subdomains: the boundary layer  $\Omega_{wg}$  (a union of curvilinear elements  $D$ , see Figure 1) and the interior polygonal region  $\Omega_{cg}$  (a union of triangular elements  $T$ ). We denote the mesh partitions

as  $\mathcal{T}_h^{wg}$  and  $\mathcal{T}_h^{cg}$ , respectively. Let  $h := \max_{K \in \mathcal{T}_h} h_K$ , where  $\mathcal{T}_h = \mathcal{T}_h^{wg} \cup \mathcal{T}_h^{cg}$ ,  $K$  can be  $D$  or  $T$ . The interface between the two regions is the boundary of a polygon denoted by  $\Gamma = \partial\Omega_{wg} \cap \partial\Omega_{cg}$ . For an integer  $k \geq 1$ , we define the continuous finite element space on the interior as:

$$V_h^{cg} = \{v_c \in C^0(\Omega_{cg}) : v_c|_T \in \mathbb{P}_k(T), \forall T \in \mathcal{T}_h^{cg}\}. \quad (24)$$

On the boundary layer, we define the weak Galerkin space as:

$$V_h^{wg} = \{v_w = (v_0, v_b) \text{ on } \Omega_{wg} : v_0|_D \in \mathbb{P}_k(D), v_b|_e \in \mathbb{P}_k|_e, e \subset \partial D, \forall D \in \mathcal{T}_h^{wg}\}, \quad (25)$$

and  $v_b$  is single-valued on WG edges. The global hybrid function space enforces strong continuity across the interface  $\Gamma$  and the zero Dirichlet boundary condition on  $\partial\Omega$ :

$$V_h = \{v = (v_c, v_w) : v_c \in V_h^{cg}, v_w \in V_h^{wg}, v_w|_\Gamma = v_b|_\Gamma = v_c|_\Gamma, v_w|_{\partial\Omega} = 0\}. \quad (26)$$

For any  $v \in V_h$ , the weak gradient  $\nabla_w v \in [\mathbb{P}_{k-1}(D)]^2$  on  $D \in \mathcal{T}_h^{wg}$  is defined by:

$$(\nabla_w v, \vec{q})_D = -(v_0, \nabla \cdot \vec{q})_D + \langle v_b, \vec{q} \cdot \mathbf{n}_{wg} \rangle_{\partial D}, \quad \forall \vec{q} \in [\mathbb{P}_{k-1}(D)]^2. \quad (27)$$

### 3.2 The Numerical Scheme

We consider the Poisson equation

$$-\Delta u = f$$

in  $\Omega$  with  $u = 0$  on  $\partial\Omega$ . The coupled WG-CG scheme seeks  $u_h = (u_c, u_w) \in V_h$  such that:

$$A_h(u_h, v) = (f, v_0)_{\Omega_{wg}} + (f, v_c)_{\Omega_{cg}}, \quad \forall v \in V_h, \quad (28)$$

where the global bilinear form is defined as:

$$A_h(u, v) = \sum_{D \in \mathcal{T}_h^{wg}} \left( (\nabla_w u_w, \nabla_w v_w)_D + s_D(u_w, v_w) \right) + \sum_{T \in \mathcal{T}_h^{cg}} (\nabla u_c, \nabla v_c)_T, \quad (29)$$

and the stabilization term on the WG elements is

$$s_D(u_w, v_w) = h_D^{-1} \langle u_0 - u_b, v_0 - v_b \rangle_{\partial D}.$$

We define the energy norm  $||| \cdot |||$  on  $V_h$  as:

$$|||v|||^2 = \sum_{D \in \mathcal{T}_h^{wg}} \left( \|\nabla_w v_w\|_{L^2(D)}^2 + s_D(v_w, v_w) \right) + \sum_{T \in \mathcal{T}_h^{cg}} \|\nabla v_c\|_{L^2(T)}^2. \quad (30)$$

**Theorem 1** (Unique Solvability). *The coupled WG-CG numerical scheme (28) has a unique solution  $u_h \in V_h$ .*

*Proof.* Since the numerical scheme (28) reduces to a square finite-dimensional linear system, it suffices to prove uniqueness. Let  $v = (v_c, v_w) \in V_h$ , with  $v_w = (v_0, v_b)$ , be the solution to the corresponding homogeneous problem (i.e., with  $f = 0$ ):

$$A_h(v, v) = 0. \quad (31)$$

By the definition of the bilinear form, this implies  $|||v|||^2 = A_h(v, v) = 0$ . Consequently, we obtain the following three conditions:

1.  $\|\nabla v_c\|_{L^2(T)} = 0$  for all  $T \in \mathcal{T}_h^{cg}$ ,
2.  $\|v_0 - v_b\|_{L^2(\partial D)} = 0 \implies v_0 = v_b$  on  $\partial D$  for all  $D \in \mathcal{T}_h^{wg}$ ,
3.  $\|\nabla_w v_w\|_{L^2(D)} = 0 \implies \nabla_w v_w = \mathbf{0}$  for all  $D \in \mathcal{T}_h^{wg}$ .

From condition 1, since  $v_c \in C^0(\Omega_{cg})$ ,  $v_c$  must be a global constant everywhere in  $\Omega_{cg}$ . On each WG element  $D$ , because  $v_0 \in \mathbb{P}_k(D)$ , we have  $\nabla v_0 \in [\mathbb{P}_{k-1}(D)]^2$ . Therefore, we can choose  $\vec{q} = \nabla v_0$  as the test function in the definition of the weak gradient to obtain:

$$0 = (\nabla_w v_w, \nabla v_0)_D = -(v_0, \Delta v_0)_D + \langle v_b, \nabla v_0 \cdot \mathbf{n}_{wg} \rangle_{\partial D}. \quad (32)$$

Applying standard integration by parts to the first term yields:

$$-(v_0, \Delta v_0)_D = (\nabla v_0, \nabla v_0)_D - \langle v_0, \nabla v_0 \cdot \mathbf{n}_{wg} \rangle_{\partial D}. \quad (33)$$

Substituting this back, we get:

$$0 = \|\nabla v_0\|_{L^2(D)}^2 - \langle v_0 - v_b, \nabla v_0 \cdot \mathbf{n}_{wg} \rangle_{\partial D}. \quad (34)$$

By condition 2 ( $v_0 = v_b$  on  $\partial D$ ), the boundary integral in (34) vanishes. Thus,  $\|\nabla v_0\|_{L^2(D)} = 0$ , which implies  $v_0$  is a constant on each element  $D$ . Since  $v_0 = v_b$  on  $\partial D$ , the boundary trace  $v_b$  shares this exact same constant value. Because  $v \in V_h$ , the function satisfies the homogeneous Dirichlet boundary condition, meaning  $v_b = 0$  on  $\partial\Omega$ . For any WG element  $D$  that shares an edge with  $\partial\Omega$ , its internal constant value must therefore be zero. By propagating this zero value across adjacent WG elements via the single-valued interfaces  $v_b$ , we find that  $v_w = (v_0, v_b) = (0, 0)$  globally throughout the boundary layer  $\Omega_{wg}$ . Finally, the space  $V_h$  enforces continuity across the interface  $\Gamma$ , yielding  $v_c|_\Gamma = v_w|_\Gamma = 0$ . Since  $v_c$  is a global constant on  $\Omega_{cg}$ , we conclude that  $v_c = 0$  everywhere in  $\Omega_{cg}$ . Therefore,  $v = 0$  over the entire domain  $\Omega$ , proving that the homogeneous problem has only the trivial solution. This guarantees the unique solvability of the scheme.  $\square$

## 4 Error Analysis

### 4.1 Global Interpolation-Projection Operator and the Error Equation

Let  $u$  be the exact solution. We define the global interpolation-projection operator  $\Pi_h u \in V_h$  as follows:

- On  $\Omega_{cg}$ ,  $\Pi_h u = I_h u$ , the standard continuous nodal interpolation of degree  $k$ .
- On  $\Omega_{wg}$ ,  $\Pi_h u|_D = Q_h u|_D = (Q_{k,D}^0 u, Q_{b,D}^\partial u)$ , where  $Q_{b,D}^\partial u$  uses the  $L^2$  projection on edges  $e \subset \partial D_{proj}$ , and the conforming nodal interpolation  $I_{k,e}^\partial u$  on the interface  $e \subset \Gamma$ .

Because  $I_{k,e}^\partial u$  perfectly matches the trace of the interior nodal interpolation  $I_h u$  on  $\Gamma$ , we have

$$Q_h u|_\Gamma = I_h u|_\Gamma,$$

ensuring  $\Pi_h u \in V_h$ .

**Lemma 6** (The Error Equation). *Let  $u \in H^{k+1}(\Omega) \cap H_0^1(\Omega)$  be the exact solution of  $-\Delta u = f$  in  $\Omega$ , and let  $u_h = (u_c, u_w) \in V_h$  solve (28). Define the global interpolation–projection  $\Pi_h u \in V_h$  by  $\Pi_h u|_{\Omega_{cg}} = I_h u$  and  $\Pi_h u|_D = Q_h u$  on each  $D \in \mathcal{T}_h^{wg}$ , and set  $e_h := \Pi_h u - u_h \in V_h$ . Then for any  $v = (v_c, v_w) \in V_h$  (with  $v_w = (v_0, v_b)$ ), we have*

$$\begin{aligned} A_h(e_h, v) &= \sum_{D \in \mathcal{T}_h^{wg}} \left\langle (\nabla u - \mathbb{Q}_{k-1,D} \nabla u) \cdot \mathbf{n}_{wg}, v_0 - v_b \right\rangle_{\partial D} + \sum_{D \in \mathcal{T}_h^{wg}} \left\langle Q_{b,D}^\partial u - u, \nabla_w v_w \cdot \mathbf{n}_{wg} \right\rangle_{\partial D} \\ &+ \sum_{D \in \mathcal{T}_h^{wg}} s_D(Q_h u, v_w) + \sum_{T \in \mathcal{T}_h^{cg}} (\nabla I_h u - \nabla u, \nabla v_c)_T. \end{aligned} \quad (35)$$

*Proof.* Fix  $v = (v_c, v_w) \in V_h$  and write  $v_w = (v_0, v_b)$  on each  $D \in \mathcal{T}_h^{wg}$ . Since  $\Pi_h u = (I_h u, Q_h u)$ , we begin by expanding

$$A_h(\Pi_h u, v) = \sum_{D \in \mathcal{T}_h^{wg}} \left( (\nabla_w Q_h u, \nabla_w v_w)_D + s_D(Q_h u, v_w) \right) + \sum_{T \in \mathcal{T}_h^{cg}} (\nabla I_h u, \nabla v_c)_T.$$

**Step 1: A local identity on each  $D \in \mathcal{T}_h^{wg}$ .** Take  $\vec{q} = \nabla_w v_w \in [\mathbb{P}_{k-1}(D)]^2$  in Lemma 5 (identity (10)) with  $\xi = u$ , to obtain

$$(\nabla_w Q_h u, \nabla_w v_w)_D = (\mathbb{Q}_{k-1,D} \nabla u, \nabla_w v_w)_D + \left\langle Q_{b,D}^\partial u - u, \nabla_w v_w \cdot \mathbf{n}_{wg} \right\rangle_{\partial D}. \quad (36)$$

By the definition of  $\nabla_w$  with test vector  $\mathbb{Q}_{k-1,D} \nabla u \in [\mathbb{P}_{k-1}(D)]^2$ , we have

$$\begin{aligned} (\mathbb{Q}_{k-1,D} \nabla u, \nabla_w v_w)_D &= -(\nabla \cdot (\mathbb{Q}_{k-1,D} \nabla u), v_0)_D + \left\langle (\mathbb{Q}_{k-1,D} \nabla u) \cdot \mathbf{n}_{wg}, v_b \right\rangle_{\partial D} \\ &= (\mathbb{Q}_{k-1,D} \nabla u, \nabla v_0)_D - \left\langle (\mathbb{Q}_{k-1,D} \nabla u) \cdot \mathbf{n}_{wg}, v_0 - v_b \right\rangle_{\partial D} \\ &= (\nabla u, \nabla v_0)_D - \left\langle (\mathbb{Q}_{k-1,D} \nabla u) \cdot \mathbf{n}_{wg}, v_0 - v_b \right\rangle_{\partial D}, \end{aligned} \quad (37)$$

where  $\nabla v_0 \in [\mathbb{P}_{k-1}(D)]^2$ . Then, using  $-\Delta u = f$  on  $D$  and integrating by parts,

$$(\nabla u, \nabla v_0)_D = (f, v_0)_D + \left\langle \nabla u \cdot \mathbf{n}_{wg}, v_0 \right\rangle_{\partial D}.$$

Replacing  $(\nabla u, \nabla v_0)_D$  by its right hand side, (37) gives

$$\begin{aligned} (\mathbb{Q}_{k-1,D} \nabla u, \nabla_w v_w)_D &= (f, v_0)_D + \left\langle \nabla u \cdot \mathbf{n}_{wg}, v_0 \right\rangle_{\partial D} - \left\langle (\mathbb{Q}_{k-1,D} \nabla u) \cdot \mathbf{n}_{wg}, v_0 - v_b \right\rangle_{\partial D} \\ &= (f, v_0)_D + \left\langle \nabla u \cdot \mathbf{n}_{wg}, v_b \right\rangle_{\partial D} + \left\langle (\nabla u - \mathbb{Q}_{k-1,D} \nabla u) \cdot \mathbf{n}_{wg}, v_0 - v_b \right\rangle_{\partial D}. \end{aligned} \quad (38)$$

Substituting (38) into (36) yields the local representation

$$\begin{aligned} (\nabla_w Q_h u, \nabla_w v_w)_D &= (f, v_0)_D + \left\langle \nabla u \cdot \mathbf{n}_{wg}, v_b \right\rangle_{\partial D} + \left\langle (\nabla u - \mathbb{Q}_{k-1,D} \nabla u) \cdot \mathbf{n}_{wg}, v_0 - v_b \right\rangle_{\partial D} \\ &+ \left\langle Q_{b,D}^\partial u - u, \nabla_w v_w \cdot \mathbf{n}_{wg} \right\rangle_{\partial D}. \end{aligned} \quad (39)$$

**Step 2: Summation over  $\mathcal{T}_h^{wg}$  and boundary/interface reduction.** Summing (39) over all  $D \in \mathcal{T}_h^{wg}$  gives

$$\begin{aligned} \sum_{D \in \mathcal{T}_h^{wg}} (\nabla_w Q_h u, \nabla_w v_w)_D &= (f, v_0)_{\Omega_{wg}} + \sum_{D \in \mathcal{T}_h^{wg}} \left\langle \nabla u \cdot \mathbf{n}_{wg}, v_b \right\rangle_{\partial D} \\ &+ \sum_{D \in \mathcal{T}_h^{wg}} \left\langle (\nabla u - \mathbb{Q}_{k-1,D} \nabla u) \cdot \mathbf{n}_{wg}, v_0 - v_b \right\rangle_{\partial D} \\ &+ \sum_{D \in \mathcal{T}_h^{wg}} \left\langle Q_{b,D}^\partial u - u, \nabla_w v_w \cdot \mathbf{n}_{wg} \right\rangle_{\partial D}. \end{aligned} \quad (40)$$

The flux term  $\sum_D \langle \nabla u \cdot \mathbf{n}_{wg}, v_b \rangle_{\partial D}$  cancels on outer-inner sides of  $D$  in  $\Omega_{wg}$  (opposite normals and single-valued traces), and  $v_b = 0$  on  $\partial\Omega$  by the definition of  $V_h$ . Hence,

$$\sum_{D \in \mathcal{T}_h^{wg}} \langle \nabla u \cdot \mathbf{n}_{wg}, v_b \rangle_{\partial D} = \langle \nabla u \cdot \mathbf{n}_{wg}, v_b \rangle_{\Gamma}. \quad (41)$$

**Step 3: The CG part and interface cancellation.** On  $\Omega_{cg}$ ,

$$\sum_{T \in \mathcal{T}_h^{cg}} (\nabla I_h u, \nabla v_c)_T = \sum_{T \in \mathcal{T}_h^{cg}} (\nabla u, \nabla v_c)_T + \sum_{T \in \mathcal{T}_h^{cg}} (\nabla I_h u - \nabla u, \nabla v_c)_T.$$

Using  $-\Delta u = f$  and integrating by parts over  $\Omega_{cg}$  (whose boundary is  $\Gamma$ ),

$$(\nabla u, \nabla v_c)_{\Omega_{cg}} = (f, v_c)_{\Omega_{cg}} + \langle \nabla u \cdot \mathbf{n}_{cg}, v_c \rangle_{\Gamma}.$$

Therefore,

$$\sum_{T \in \mathcal{T}_h^{cg}} (\nabla I_h u, \nabla v_c)_T = (f, v_c)_{\Omega_{cg}} + \langle \nabla u \cdot \mathbf{n}_{cg}, v_c \rangle_{\Gamma} + \sum_{T \in \mathcal{T}_h^{cg}} (\nabla I_h u - \nabla u, \nabla v_c)_T. \quad (42)$$

On the interface  $\Gamma$ , the outward normals satisfy  $\mathbf{n}_{wg} = -\mathbf{n}_{cg}$  and  $v \in V_h$  enforces  $v_b = v_c$  on  $\Gamma$ . Hence,

$$\langle \nabla u \cdot \mathbf{n}_{wg}, v_b \rangle_{\Gamma} + \langle \nabla u \cdot \mathbf{n}_{cg}, v_c \rangle_{\Gamma} = 0.$$

**Step 4: Assemble  $A_h(\Pi_h u, v)$  and subtract the discrete scheme.** Insert (40)–(41) and (42) into the expansion of  $A_h(\Pi_h u, v)$ . After the interface cancellation, we obtain

$$\begin{aligned} A_h(\Pi_h u, v) &= (f, v_0)_{\Omega_{wg}} + (f, v_c)_{\Omega_{cg}} + \sum_{D \in \mathcal{T}_h^{wg}} \langle (\nabla u - \mathbb{Q}_{k-1,D} \nabla u) \cdot \mathbf{n}_{wg}, v_0 - v_b \rangle_{\partial D} \\ &\quad + \sum_{D \in \mathcal{T}_h^{wg}} \langle \mathbb{Q}_{b,D}^\partial u - u, \nabla_w v_w \cdot \mathbf{n}_{wg} \rangle_{\partial D} + \sum_{D \in \mathcal{T}_h^{wg}} s_D(Q_h u, v_w) + \sum_{T \in \mathcal{T}_h^{cg}} (\nabla I_h u - \nabla u, \nabla v_c)_T. \end{aligned}$$

Finally, subtract the discrete equation (28),  $A_h(u_h, v) = (f, v_0)_{\Omega_{wg}} + (f, v_c)_{\Omega_{cg}}$ , to get (35) with  $e_h = \Pi_h u - u_h$ .  $\square$

## 4.2 Energy Norm Estimate

We first record two local approximation facts that hold on each shape-regular curvilinear element  $D \in \mathcal{T}_h^{wg}$  (star-shaped with uniform chunkiness), and on each  $T \in \mathcal{T}_h^{cg}$ . They follow from the averaged Taylor polynomial (Bramble–Hilbert) argument on  $D$  and standard Lagrange interpolation theory on  $T$ .

**Lemma 7** (Local approximation estimates). *Let  $k \geq 1$  and  $u \in H^{k+1}(D)$ .*

$$\|u - Q_{k,D}^0 u\|_{L^2(D)} + h_D \|\nabla(u - Q_{k,D}^0 u)\|_{L^2(D)} \lesssim h_D^{k+1} \|u\|_{H^{k+1}(D)}, \quad (43)$$

$$\|\nabla u - \mathbb{Q}_{k-1,D} \nabla u\|_{L^2(D)} + h_D \|\nabla(\nabla u - \mathbb{Q}_{k-1,D} \nabla u)\|_{L^2(D)} \lesssim h_D^k \|u\|_{H^{k+1}(D)}. \quad (44)$$

Moreover, for any side  $e \subset \partial D$ ,

$$\|u - Q_{k,D}^0 u\|_{L^2(e)} \lesssim h_D^{k+1/2} \|u\|_{H^{k+1}(D)}, \quad (45)$$

$$\|(\nabla u - \mathbb{Q}_{k-1,D} \nabla u) \cdot \mathbf{n}_{wg}\|_{L^2(e)} \lesssim h_D^{k-1/2} \|u\|_{H^{k+1}(D)}. \quad (46)$$

Finally, on each  $T \in \mathcal{T}_h^{cg}$ ,

$$\|\nabla(u - I_h u)\|_{L^2(T)} \lesssim h_T^k \|u\|_{H^{k+1}(T)}. \quad (47)$$

*Proof.* The volume estimates (43)–(44) follow by taking the averaged Taylor polynomial  $p \in \mathbb{P}_k(D)$  (respectively  $\vec{p} \in [\mathbb{P}_{k-1}(D)]^2$  for  $\nabla u$ ) as an approximant and then using the best-approximation property of  $L^2$ -projections together with the Bramble–Hilbert bounds on star-shaped domains. The boundary estimates (45)–(46) follow from the trace inequality on  $D$  applied to  $u - Q_{k,D}^0 u$  and to  $(\nabla u - \mathbb{Q}_{k-1,D} \nabla u) \cdot \mathbf{n}_{wg}$ , using the corresponding volume bounds. The interpolation estimate (47) is standard for  $C^0$  Lagrange elements on triangles.  $\square$

**Lemma 8** (Stabilization consistency on  $D$ ). *Let  $Q_h u|_D = (Q_{k,D}^0 u, Q_{b,D}^\partial u)$  be the mixed interpolation–projection operator. Then for  $u \in H^{k+1}(D)$ ,*

$$s_D(Q_h u, Q_h u)^{1/2} = h_D^{-1/2} \|Q_{k,D}^0 u - Q_{b,D}^\partial u\|_{L^2(\partial D)} \lesssim h_D^k \|u\|_{H^{k+1}(D)}. \quad (48)$$

*Proof.* By the triangle inequality,

$$\|Q_{k,D}^0 u - Q_{b,D}^\partial u\|_{L^2(\partial D)} \leq \|Q_{k,D}^0 u - u\|_{L^2(\partial D)} + \|u - Q_{b,D}^\partial u\|_{L^2(\partial D)}.$$

The first term is bounded by (45) from Lemma 7.

For the second term, on each edge  $e \subset \partial D$  we have either: (i)  $Q_{b,D}^\partial = Q_{k,e}^\partial$  ( $L^2$ -projection), so

$$\|u - Q_{b,D}^\partial u\|_{L^2(e)} \leq \|u - p\|_{L^2(e)} \lesssim h_D^{k+1/2} \|u\|_{H^{k+1}(D)}$$

using the same averaged Taylor polynomial  $p \in \mathbb{P}_k(D)$  and the trace estimate; or (ii)  $Q_{b,D}^\partial = I_{k,e}^\partial$  (nodal interpolant), and the bound

$$\|u - I_{k,e}^\partial u\|_{L^2(e)} \lesssim h_D^{k+1/2} \|u\|_{H^{k+1}(D)}$$

follows from the same argument as in Lemma 5 from (19) to (20), using the stability of  $I_{k,e}^\partial$  and the  $L^\infty$  bound for  $u - p$  provided by Lemma 3, which follows from the averaged Taylor polynomial estimate together with the Sobolev embedding  $H^{k+1}(D) \hookrightarrow L^\infty(D)$  for  $k \geq 1$  in two dimensions. Summing over all sides of  $\partial D$  yields

$$\|u - Q_{b,D}^\partial u\|_{L^2(\partial D)} \lesssim h_D^{k+1/2} \|u\|_{H^{k+1}(D)}. \quad (49)$$

Multiplying by  $h_D^{-1/2}$  proves (48).  $\square$

**Theorem 2** (Energy norm estimate). *Let  $k \geq 1$  and assume  $u \in H^{k+1}(\Omega) \cap H_0^1(\Omega)$  solves  $-\Delta u = f$  in  $\Omega$ . Let  $u_h \in V_h$  solve the coupled WG–CG scheme (28), and let  $\Pi_h u \in V_h$  be the global interpolation–projection operator. Then there exists a constant  $C > 0$ , independent of  $h$ , such that*

$$||| \Pi_h u - u_h ||| \leq C h^k \|u\|_{H^{k+1}(\Omega)}. \quad (50)$$

*Proof.* Set  $e_h := \Pi_h u - u_h \in V_h$ . Taking  $v = e_h$  in the error equation (35) gives

$$\begin{aligned} |||e_h|||^2 &= \sum_{D \in \mathcal{T}_h^{wg}} \left\langle (\nabla u - \mathbb{Q}_{k-1,D} \nabla u) \cdot \mathbf{n}_{wg}, e_0 - e_b \right\rangle_{\partial D} + \sum_{D \in \mathcal{T}_h^{wg}} \left\langle Q_{b,D}^\partial u - u, \nabla_w e_w \cdot \mathbf{n}_{wg} \right\rangle_{\partial D} \\ &\quad + \sum_{D \in \mathcal{T}_h^{wg}} s_D(Q_h u, e_w) + \sum_{T \in \mathcal{T}_h^{cg}} (\nabla I_h u - \nabla u, \nabla e_c)_T \\ &=: J_1 + J_2 + J_3 + J_4. \end{aligned}$$

We estimate each term by  $Ch^k \|u\|_{H^{k+1}(\Omega)} |||e_h|||$ .

**Estimate of  $J_1$ .** By Cauchy–Schwarz and (46) from Lemma 7,

$$|J_1| \leq \sum_D \|(\nabla u - \mathbb{Q}_{k-1,D} \nabla u) \cdot \mathbf{n}_{wg}\|_{L^2(\partial D)} \|e_0 - e_b\|_{L^2(\partial D)} \lesssim \sum_D h_D^{k-1/2} \|u\|_{H^{k+1}(D)} \|e_0 - e_b\|_{L^2(\partial D)}.$$

Using  $s_D(e_w, e_w) = h_D^{-1} \|e_0 - e_b\|_{L^2(\partial D)}^2$ , we have  $\|e_0 - e_b\|_{L^2(\partial D)} = h_D^{1/2} s_D(e_w, e_w)^{1/2}$ , hence

$$|J_1| \lesssim \sum_D h_D^k \|u\|_{H^{k+1}(D)} s_D(e_w, e_w)^{1/2} \leq \left( \sum_D h_D^{2k} \|u\|_{H^{k+1}(D)}^2 \right)^{1/2} \left( \sum_D s_D(e_w, e_w) \right)^{1/2}.$$

Then  $\sum_D h_D^{2k} \|u\|_{H^{k+1}(D)}^2 \leq h^{2k} \|u\|_{H^{k+1}(\Omega_{wg})}^2$ , and  $(\sum_D s_D(e_w, e_w))^{1/2} \leq \|e_h\|$ . Therefore

$$|J_1| \lesssim h^k \|u\|_{H^{k+1}(\Omega_{wg})} \|e_h\| \leq h^k \|u\|_{H^{k+1}(\Omega)} \|e_h\|. \quad (51)$$

**Estimate of  $J_2$ .** Apply Lemma 5 (11) with  $\xi = u$  and  $\vec{q} = \nabla_w e_w \in [\mathbb{P}_{k-1}(D)]^2$  to obtain, on each  $D$ ,

$$\left| \langle Q_{b,D}^\partial u - u, \nabla_w e_w \cdot \mathbf{n}_{wg} \rangle_{\partial D} \right| \lesssim h_D^k \|u\|_{H^{k+1}(D)} \|\nabla_w e_w\|_{L^2(D)}.$$

Summing over  $D$  and using Cauchy–Schwarz gives

$$|J_2| \lesssim h^k \|u\|_{H^{k+1}(\Omega_{wg})} \left( \sum_D \|\nabla_w e_w\|_{L^2(D)}^2 \right)^{1/2} \leq h^k \|u\|_{H^{k+1}(\Omega_{wg})} \|e_h\|. \quad (52)$$

**Estimate of  $J_3$ .** By Cauchy–Schwarz in the stabilization inner product,

$$|J_3| = \left| \sum_D s_D(Q_h u, e_w) \right| \leq \left( \sum_D s_D(Q_h u, Q_h u) \right)^{1/2} \left( \sum_D s_D(e_w, e_w) \right)^{1/2}.$$

Using Lemma 8 and  $h_D \leq h$ ,

$$\left( \sum_D s_D(Q_h u, Q_h u) \right)^{1/2} \lesssim \left( \sum_D h_D^{2k} \|u\|_{H^{k+1}(D)}^2 \right)^{1/2} \leq h^k \|u\|_{H^{k+1}(\Omega_{wg})}.$$

Also  $(\sum_D s_D(e_w, e_w))^{1/2} \leq \|e_h\|$ . Hence

$$|J_3| \lesssim h^k \|u\|_{H^{k+1}(\Omega)} \|e_h\|. \quad (53)$$

**Estimate of  $J_4$ .** By Cauchy–Schwarz and the interpolation estimate (47),

$$|J_4| \leq \left( \sum_T \|\nabla(I_h u - u)\|_{L^2(T)}^2 \right)^{1/2} \left( \sum_T \|\nabla e_c\|_{L^2(T)}^2 \right)^{1/2} \lesssim h^k \|u\|_{H^{k+1}(\Omega_{cg})} \|e_h\| \leq h^k \|u\|_{H^{k+1}(\Omega)} \|e_h\|.$$

Thus,

$$|J_4| \lesssim h^k \|u\|_{H^{k+1}(\Omega)} \|e_h\|. \quad (54)$$

**Conclusion.** Combining (51)–(54) yields

$$\|e_h\|^2 \leq C h^k \|u\|_{H^{k+1}(\Omega)} \|e_h\|.$$

If  $\|e_h\| = 0$  the claim is trivial; otherwise divide both sides by  $\|e_h\|$  to obtain (50). This completes the proof.  $\square$

### 4.3 $L^2$ Norm Estimate

For  $e_h = (e_c, e_w) \in V_h$  with  $e_w = (e_0, e_b)$ , define the piecewise scalar error

$$e_h^*(x) := \begin{cases} e_0(x), & x \in \Omega_{wg}, \\ e_c(x), & x \in \Omega_{cg}. \end{cases} \quad \text{so that} \quad \|e_h^*\|_{L^2(\Omega)}^2 = \|e_0\|_{L^2(\Omega_{wg})}^2 + \|e_c\|_{L^2(\Omega_{cg})}^2.$$

The energy-norm estimate above uses only the geometric assumptions on the mesh and local approximation properties. To derive the  $L^2$  estimate, we additionally assume the usual elliptic regularity on the curved domain: for any  $\Psi \in L^2(\Omega)$ , the solution  $\Phi \in H_0^1(\Omega)$  of  $-\Delta\Phi = \Psi$  satisfies

$$\|\Phi\|_{H^2(\Omega)} \lesssim \|\Psi\|_{L^2(\Omega)}. \quad (55)$$

A sufficient condition for this elliptic regularity is that the boundary is  $C^{1,1}$ .

**Theorem 3.** *Assume (55). Let  $u \in H^{k+1}(\Omega) \cap H_0^1(\Omega)$  solve  $-\Delta u = f$  in  $\Omega$  and let  $u_h \in V_h$  solve (28). Let  $e_h = \Pi_h u - u_h$  and define  $e_h^*$  as above. Then there exists  $C > 0$ , independent of  $h$ , such that*

$$\|e_h^*\|_{L^2(\Omega)} \leq C h^{k+1} \|u\|_{H^{k+1}(\Omega)}. \quad (56)$$

*Proof.* Let  $\Phi \in H_0^1(\Omega) \cap H^2(\Omega)$  solve the dual problem

$$-\Delta\Phi = e_h^* \quad \text{in } \Omega, \quad \Phi = 0 \quad \text{on } \partial\Omega. \quad (57)$$

Let  $\Pi_h\Phi \in V_h$  be the global interpolation-projection defined by  $\Pi_h\Phi|_{\Omega_{cg}} = I_h\Phi$  and  $\Pi_h\Phi|_D = Q_h\Phi = (Q_{k,D}^0\Phi, Q_{b,D}^\partial\Phi)$  on each  $D \in \mathcal{T}_h^{wg}$ .

**Step 1: A duality identity**  $\|e_h^*\|^2 = A_h(e_h, \Pi_h\Phi) + \mathcal{R}(\Phi; e_h)$ . By (57),

$$\|e_h^*\|_{L^2(\Omega)}^2 = (-\Delta\Phi, e_0)_{\Omega_{wg}} + (-\Delta\Phi, e_c)_{\Omega_{cg}}.$$

Integrating by parts elementwise on  $\Omega_{wg}$  and once on  $\Omega_{cg}$  yields

$$\|e_h^*\|_{L^2(\Omega)}^2 = \sum_{D \in \mathcal{T}_h^{wg}} (\nabla\Phi, \nabla e_0)_D - \sum_{D \in \mathcal{T}_h^{wg}} \langle \nabla\Phi \cdot \mathbf{n}_{wg}, e_0 \rangle_{\partial D} + (\nabla\Phi, \nabla e_c)_{\Omega_{cg}} - \langle \nabla\Phi \cdot \mathbf{n}_{cg}, e_c \rangle_\Gamma. \quad (58)$$

Rewrite  $\langle \nabla\Phi \cdot \mathbf{n}_{wg}, e_0 \rangle_{\partial D} = \langle \nabla\Phi \cdot \mathbf{n}_{wg}, e_b \rangle_{\partial D} + \langle \nabla\Phi \cdot \mathbf{n}_{wg}, e_0 - e_b \rangle_{\partial D}$  and sum over  $D$ . The terms with  $e_b$  cancel on interior WG edges and vanish on  $\partial\Omega$ ; thus  $\sum_D \langle \nabla\Phi \cdot \mathbf{n}_{wg}, e_b \rangle_{\partial D} = \langle \nabla\Phi \cdot \mathbf{n}_{wg}, e_b \rangle_\Gamma$ . Since  $\mathbf{n}_{wg} = -\mathbf{n}_{cg}$  on  $\Gamma$  and  $e_b = e_c$  on  $\Gamma$  (because  $e_h \in V_h$ ), the interface fluxes cancel:

$$\langle \nabla\Phi \cdot \mathbf{n}_{wg}, e_b \rangle_\Gamma + \langle \nabla\Phi \cdot \mathbf{n}_{cg}, e_c \rangle_\Gamma = 0.$$

Therefore (58) reduces to

$$\|e_h^*\|_{L^2(\Omega)}^2 = \sum_D (\nabla\Phi, \nabla e_0)_D - \sum_D \langle \nabla\Phi \cdot \mathbf{n}_{wg}, e_0 - e_b \rangle_{\partial D} + (\nabla\Phi, \nabla e_c)_{\Omega_{cg}}. \quad (59)$$

Now fix  $D \in \mathcal{T}_h^{wg}$  and write  $\mathbb{Q}_{k-1,D}$  for the  $L^2(D)$ -projection onto  $[\mathbb{P}_{k-1}(D)]^2$ . Split  $\nabla\Phi = \mathbb{Q}_{k-1,D}\nabla\Phi + (\nabla\Phi - \mathbb{Q}_{k-1,D}\nabla\Phi)$  and use the identity (valid for any  $\vec{q} \in [\mathbb{P}_{k-1}(D)]^2$ )

$$(\nabla_w e_w, \vec{q})_D = (\nabla e_0, \vec{q})_D - \langle e_0 - e_b, \vec{q} \cdot \mathbf{n}_{wg} \rangle_{\partial D}, \quad (60)$$

which follows directly from the definition of  $\nabla_w$  by integrating  $(e_0, \nabla \cdot \vec{q})_D$  by parts.

Taking  $\vec{q} = \mathbb{Q}_{k-1,D} \nabla \Phi$  in (60) and inserting into (59) gives

$$\begin{aligned} \|e_h^*\|_{L^2(\Omega)}^2 &= \sum_D (\nabla_w e_w, \mathbb{Q}_{k-1,D} \nabla \Phi)_D + \sum_D (\nabla e_0, \nabla \Phi - \mathbb{Q}_{k-1,D} \nabla \Phi)_D \\ &\quad - \sum_D \langle (\nabla \Phi - \mathbb{Q}_{k-1,D} \nabla \Phi) \cdot \mathbf{n}_{wg}, e_0 - e_b \rangle_{\partial D} \\ &\quad + (\nabla I_h \Phi, \nabla e_c)_{\Omega_{cg}} + (\nabla(\Phi - I_h \Phi), \nabla e_c)_{\Omega_{cg}}. \end{aligned} \quad (61)$$

Since  $e_0|_D \in \mathbb{P}_k(D)$ , its gradient satisfies  $\nabla e_0 \in [\mathbb{P}_{k-1}(D)]^2$ . By the definition of the  $L^2$  projection  $\mathbb{Q}_{k-1,D}$ , the second term vanishes identically:

$$\sum_D (\nabla e_0, \nabla \Phi - \mathbb{Q}_{k-1,D} \nabla \Phi)_D = 0. \quad (62)$$

Next, apply Lemma 5 (identity (10)) to  $\xi = \Phi$  with  $\vec{q} = \nabla_w e_w \in [\mathbb{P}_{k-1}(D)]^2$ :

$$(\nabla_w Q_h \Phi, \nabla_w e_w)_D = (\mathbb{Q}_{k-1,D} \nabla \Phi, \nabla_w e_w)_D + \langle Q_{b,D}^\partial \Phi - \Phi, \nabla_w e_w \cdot \mathbf{n}_{wg} \rangle_{\partial D},$$

hence

$$(\nabla_w e_w, \mathbb{Q}_{k-1,D} \nabla \Phi)_D = (\nabla_w e_w, \nabla_w Q_h \Phi)_D - \langle Q_{b,D}^\partial \Phi - \Phi, \nabla_w e_w \cdot \mathbf{n}_{wg} \rangle_{\partial D}.$$

Insert this into (61) and add/subtract the stabilization term to identify  $A_h$ :

$$\|e_h^*\|_{L^2(\Omega)}^2 = A_h(e_h, \Pi_h \Phi) + \mathcal{R}(\Phi; e_h), \quad (63)$$

where the remainder  $\mathcal{R}(\Phi; e_h)$  drops the zero term (62) and is simply given by

$$\begin{aligned} \mathcal{R}(\Phi; e_h) &:= - \sum_D \langle (\nabla \Phi - \mathbb{Q}_{k-1,D} \nabla \Phi) \cdot \mathbf{n}_{wg}, e_0 - e_b \rangle_{\partial D} \\ &\quad - \sum_D \langle Q_{b,D}^\partial \Phi - \Phi, \nabla_w e_w \cdot \mathbf{n}_{wg} \rangle_{\partial D} \\ &\quad + (\nabla(\Phi - I_h \Phi), \nabla e_c)_{\Omega_{cg}} - \sum_D s_D(e_w, Q_h \Phi). \end{aligned} \quad (64)$$

**Step 2: Bound the remainder  $\mathcal{R}(\Phi; e_h)$ .** We claim

$$|\mathcal{R}(\Phi; e_h)| \lesssim h \|\Phi\|_{H^2(\Omega)} \|e_h\|. \quad (65)$$

Because  $\Phi \in H^2(\Omega)$ , by Lemmas 7–8 and (49), we have the following approximation estimates:

$$\begin{aligned} \|(\nabla \Phi - \mathbb{Q}_{k-1,D} \nabla \Phi) \cdot \mathbf{n}_{wg}\|_{L^2(\partial D)} &\lesssim h_D^{1/2} \|\Phi\|_{H^2(D)}, \\ \|Q_{b,D}^\partial \Phi - \Phi\|_{L^2(\partial D)} &\lesssim h_D^{3/2} \|\Phi\|_{H^2(D)}, \\ s_D(Q_h \Phi, Q_h \Phi)^{1/2} &\lesssim h_D \|\Phi\|_{H^2(D)}, \\ \|\nabla(\Phi - I_h \Phi)\|_{L^2(\Omega_{cg})} &\lesssim h \|\Phi\|_{H^2(\Omega)}. \end{aligned}$$

Using these facts, each term in (64) is bounded as follows:

- For the first term, we write  $h_D^{-1/2} \|e_0 - e_b\|_{L^2(\partial D)} = s_D(e_w, e_w)^{1/2}$  and bound it by the energy norm.

- For the second term, apply the inverse trace inequality for polynomials to get  $\|\nabla_w e_w \cdot \mathbf{n}_{wg}\|_{L^2(\partial D)} \lesssim h_D^{-1/2} \|\nabla_w e_w\|_{L^2(D)}$  and multiply by the  $h_D^{3/2}$  bound.
- The third and fourth terms are directly bounded using Cauchy–Schwarz and the definition of the energy norm.

Summing over all elements yields  $|\mathcal{R}(\Phi; e_h)| \leq Ch \|\Phi\|_{H^2(\Omega)} \|e_h\|$ .

**Step 3: Bound  $A_h(e_h, \Pi_h \Phi)$  using the error equation and interface cancellation.** Apply the error equation (35) with  $v = \Pi_h \Phi$  to obtain

$$\begin{aligned}
A_h(e_h, \Pi_h \Phi) &= \sum_D \left\langle (\nabla u - \mathbb{Q}_{k-1,D} \nabla u) \cdot \mathbf{n}_{wg}, Q_{k,D}^0 \Phi - Q_{b,D}^\partial \Phi \right\rangle_{\partial D} \\
&\quad + \sum_D \left\langle Q_{b,D}^\partial u - u, \nabla_w Q_h \Phi \cdot \mathbf{n}_{wg} \right\rangle_{\partial D} \\
&\quad + \sum_D s_D(Q_h u, Q_h \Phi) + (\nabla I_h u - \nabla u, \nabla I_h \Phi)_{\Omega_{cg}}. \tag{66}
\end{aligned}$$

The first and third terms are estimated directly:

$$\begin{aligned}
\left| \sum_D \left\langle (\nabla u - \mathbb{Q}_{k-1,D} \nabla u) \cdot \mathbf{n}_{wg}, Q_{k,D}^0 \Phi - Q_{b,D}^\partial \Phi \right\rangle_{\partial D} \right| &\lesssim \sum_D (h_D^{k-1/2} \|u\|_{H^{k+1}(D)}) (h_D^{3/2} \|\Phi\|_{H^2(D)}) \\
&\lesssim h^{k+1} \|u\|_{H^{k+1}(\Omega)} \|\Phi\|_{H^2(\Omega)},
\end{aligned}$$

and

$$\begin{aligned}
\left| \sum_D s_D(Q_h u, Q_h \Phi) \right| &\leq \left( \sum_D s_D(Q_h u, Q_h u) \right)^{1/2} \left( \sum_D s_D(Q_h \Phi, Q_h \Phi) \right)^{1/2} \\
&\lesssim (h^k \|u\|_{H^{k+1}(\Omega)}) (h \|\Phi\|_{H^2(\Omega)}) \lesssim h^{k+1} \|u\|_{H^{k+1}(\Omega)} \|\Phi\|_{H^2(\Omega)}.
\end{aligned}$$

For the remaining two terms in (66), we *do not* bound them separately; instead, we combine them to exploit cancellation on the interface  $\Gamma$ .

(a) *Reduce the WG boundary term to  $\Gamma$ .* We split the boundary  $\partial D_{proj}$  into straight outer-inner edges (which are internal to the domain) and curved outer edges (which lie on  $\partial\Omega$ ). On any straight edge  $e \subset \partial D_{proj} \setminus \partial\Omega$ , the normal vector  $\mathbf{n}_{wg}$  is constant. Since  $\nabla_w Q_h \Phi \in [\mathbb{P}_{k-1}(D)]^2$ , its normal trace  $\nabla_w Q_h \Phi \cdot \mathbf{n}_{wg}|_e$  is a polynomial in  $\mathbb{P}_{k-1}(e) \subset \mathbb{P}_k(e)$ . Because  $Q_{b,D}^\partial$  is the  $L^2(e)$ -projection onto  $\mathbb{P}_k(e)$ , by orthogonality we have:

$$\langle Q_{b,D}^\partial u - u, \nabla_w Q_h \Phi \cdot \mathbf{n}_{wg} \rangle_e = 0, \quad e \subset \partial D_{proj} \setminus \partial\Omega.$$

On the other hand, for any curved edge  $e \subset \partial D_{proj} \cap \partial\Omega$ , the homogeneous Dirichlet boundary condition requires  $u = 0$ . Consequently,  $Q_{b,D}^\partial u = 0$ , making the integral trivially zero on  $\partial\Omega$ .

Hence, the only non-vanishing contribution comes from the interface  $\Gamma$  (where  $e \subset \partial D_{int}$ ):

$$\sum_D \left\langle Q_{b,D}^\partial u - u, \nabla_w Q_h \Phi \cdot \mathbf{n}_{wg} \right\rangle_{\partial D} = \left\langle I_h u - u, \nabla_w Q_h \Phi \cdot \mathbf{n}_{wg} \right\rangle_{\Gamma}, \tag{67}$$

because on  $\Gamma$  we defined  $Q_{b,D}^\partial u = I_{k,e}^\partial u = I_h u|_{\Gamma}$ .

(b) *Split the CG term and integrate by parts to produce a cancelling interface flux.* Write

$$(\nabla I_h u - \nabla u, \nabla I_h \Phi)_{\Omega_{cg}} = (\nabla I_h u - \nabla u, \nabla(I_h \Phi - \Phi))_{\Omega_{cg}} + (\nabla I_h u - \nabla u, \nabla \Phi)_{\Omega_{cg}}. \tag{68}$$

The first term is bounded by interpolation:

$$|(\nabla I_h u - \nabla u, \nabla(I_h \Phi - \Phi))_{\Omega_{cg}}| \lesssim (h^k \|u\|_{H^{k+1}(\Omega)})(h \|\Phi\|_{H^2(\Omega)}) \lesssim h^{k+1} \|u\|_{H^{k+1}(\Omega)} \|\Phi\|_{H^2(\Omega)}.$$

For the second term, integrate by parts on  $\Omega_{cg}$  (whose outward normal is  $\mathbf{n}_{cg} = -\mathbf{n}_{wg}$ ):

$$\begin{aligned} (\nabla I_h u - \nabla u, \nabla \Phi)_{\Omega_{cg}} &= -(I_h u - u, \Delta \Phi)_{\Omega_{cg}} + \langle I_h u - u, \nabla \Phi \cdot \mathbf{n}_{cg} \rangle_{\Gamma} \\ &= (I_h u - u, e_h^*)_{\Omega_{cg}} - \langle I_h u - u, \nabla \Phi \cdot \mathbf{n}_{wg} \rangle_{\Gamma}, \end{aligned} \quad (69)$$

where we used  $-\Delta \Phi = e_h^*$  and  $\mathbf{n}_{cg} = -\mathbf{n}_{wg}$ .

Now combine the interface flux in (69) with (67):

$$\left\langle I_h u - u, \nabla_w Q_h \Phi \cdot \mathbf{n}_{wg} \right\rangle_{\Gamma} - \left\langle I_h u - u, \nabla \Phi \cdot \mathbf{n}_{wg} \right\rangle_{\Gamma} = \left\langle I_h u - u, (\nabla_w Q_h \Phi - \nabla \Phi) \cdot \mathbf{n}_{wg} \right\rangle_{\Gamma}. \quad (70)$$

Using the inverse trace inequality and Lemma 5 (estimate (12) applied to  $\xi = \Phi \in H^2$  gives  $\|\nabla_w Q_h \Phi - \mathbb{Q}_{k-1,D} \nabla \Phi\|_{L^2(D)} \lesssim h_D \|\Phi\|_{H^2(D)}$ ), together with  $\|\nabla \Phi - \mathbb{Q}_{k-1,D} \nabla \Phi\|_{L^2(D)} \lesssim h_D \|\Phi\|_{H^2(D)}$ , we obtain

$$\|(\nabla_w Q_h \Phi - \nabla \Phi) \cdot \mathbf{n}_{wg}\|_{L^2(\Gamma)} \lesssim h^{1/2} \|\Phi\|_{H^2(\Omega)}. \quad (71)$$

Therefore, using  $\|I_h u - u\|_{L^2(\Gamma)} \lesssim h^{k+1/2} \|u\|_{H^{k+1}(\Omega)}$ ,

$$\left| \langle I_h u - u, (\nabla_w Q_h \Phi - \nabla \Phi) \cdot \mathbf{n}_{wg} \rangle_{\Gamma} \right| \lesssim h^{k+1} \|u\|_{H^{k+1}(\Omega)} \|\Phi\|_{H^2(\Omega)}. \quad (72)$$

Finally, from (69),

$$|(I_h u - u, e_h^*)_{\Omega_{cg}}| \leq \|I_h u - u\|_{L^2(\Omega_{cg})} \|e_h^*\|_{L^2(\Omega)} \lesssim h^{k+1} \|u\|_{H^{k+1}(\Omega)} \|e_h^*\|_{L^2(\Omega)}. \quad (73)$$

Collecting all bounds for the four terms in (66) (using (67), (68)–(73)), we obtain

$$|A_h(e_h, \Pi_h \Phi)| \lesssim h^{k+1} \|u\|_{H^{k+1}(\Omega)} \left( \|\Phi\|_{H^2(\Omega)} + \|e_h^*\|_{L^2(\Omega)} \right). \quad (74)$$

**Step 4: Conclude the  $L^2$  estimate.** Insert (74) and (65) into (63):

$$\|e_h^*\|_{L^2(\Omega)}^2 \lesssim h^{k+1} \|u\|_{H^{k+1}(\Omega)} \left( \|\Phi\|_{H^2(\Omega)} + \|e_h^*\|_{L^2(\Omega)} \right) + h \|\Phi\|_{H^2(\Omega)} \|e_h\|.$$

Using the energy estimate  $\|e_h\| \lesssim h^k \|u\|_{H^{k+1}(\Omega)}$  (Theorem 2) and the dual regularity (55) with  $\Psi = e_h^*$  (so  $\|\Phi\|_{H^2(\Omega)} \lesssim \|e_h^*\|_{L^2(\Omega)}$ ), we arrive at

$$\|e_h^*\|_{L^2(\Omega)}^2 \lesssim h^{k+1} \|u\|_{H^{k+1}(\Omega)} \|e_h^*\|_{L^2(\Omega)}.$$

If  $\|e_h^*\|_{L^2(\Omega)} = 0$  we are done; otherwise divide by  $\|e_h^*\|_{L^2(\Omega)}$  to obtain (56).  $\square$

## 5 Numerical Experiments

This section verifies the convergence theory for the coupled WG–CG method on curved domains. All computations are performed on a unit disk

$$\Omega = \{(x, y) \in \mathbb{R}^2 : x^2 + y^2 < 1\},$$

with a boundary-layer mesh: a collection of curvilinear WG elements adjacent to  $\partial\Omega$ , and a polygonal interior region triangulated for the conforming CG method.

**Meshes.** Let  $R_{\text{out}}$  and  $R_{\text{in}}$  denote the outer and inner radii of the boundary layer, respectively. Since the computational domain is the unit disk, we set  $R_{\text{out}} = 1$  and  $R_{\text{in}} = 1 - H$ , so that

$$H := R_{\text{out}} - R_{\text{in}}$$

is exactly the boundary-layer thickness. The interface  $\Gamma$  is a regular  $N_\theta$ -gon with

$$N_\theta \approx \left\lfloor \frac{2\pi}{H} \right\rfloor,$$

generated by connecting vertices on the circle of radius  $R_{\text{in}}$ . Each WG element  $D$  is bounded by one outer circular arc on  $\partial\Omega$ , two radial segments, and one inner chord (edge on  $\Gamma$ ). The interior  $\Omega_{cg}$  is triangulated by a Delaunay triangulation of the interior nodes. For each refinement,  $H$  is decreased by half,  $H$  starts from 0.1, see Figure 2.

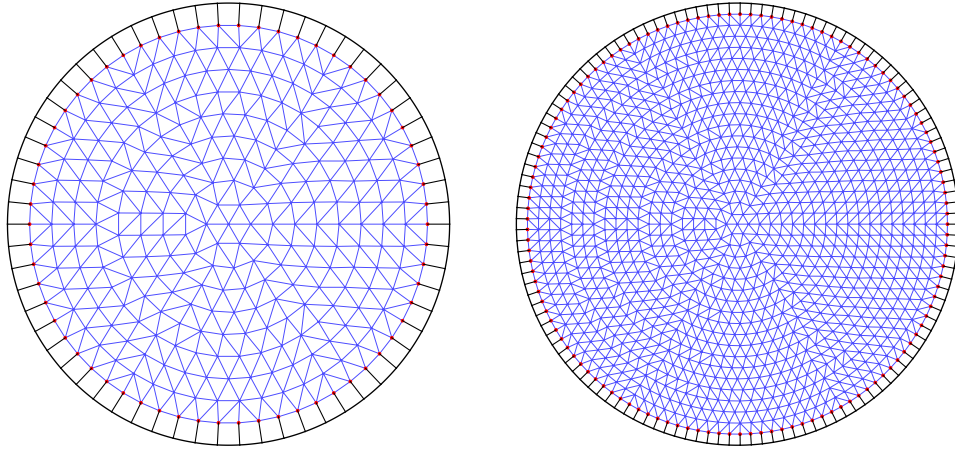


Figure 2: The coupled mesh for Continuous Galerkin and Weak Galerkin. **Left:** a coarse mesh,  $H = 0.1$ . **Right:** a refined mesh,  $H = 0.05$ . Red dots are interface points. The numerical solution is continuous in the CG region (triangles) but discontinuous in the WG region (curvilinear polygons). As the mesh is refined, the boundary layer becomes thinner.

**Error metrics and empirical rates.** Let  $u$  be the exact solution and  $u_h = (u_c, u_w) \in V_h$  be the discrete solution. We report the energy-norm error

$$\| \Pi_h u - u_h \|_{\text{energy}}^2 = \sum_{D \in \mathcal{T}_h^{wg}} \left( \|\nabla_w(\Pi_h u - u_h)\|_{L^2(D)}^2 + s_D(\Pi_h u - u_h, \Pi_h u - u_h) \right) + \sum_{T \in \mathcal{T}_h^{cg}} \|\nabla(\Pi_h u - u_h)\|_{L^2(T)}^2,$$

and the  $L^2$ -error of the piecewise scalar field

$$u_h^*(x) = \begin{cases} (u_h)_0(x), & x \in \Omega_{wg}, \\ u_c(x), & x \in \Omega_{cg}, \end{cases} \quad \text{so that} \quad \|u - u_h^*\|_{L^2(\Omega)}^2 = \|u - (u_h)_0\|_{L^2(\Omega_{wg})}^2 + \|u - u_c\|_{L^2(\Omega_{cg})}^2.$$

Given a refinement sequence  $\{H_\ell\}$  and the errors  $\{E_{H_\ell}\}$ , the empirical rate is computed by

$$\text{rate} = \frac{\log(E_{H_\ell}/E_{H_{\ell+1}})}{\log(H_\ell/H_{\ell+1})} \quad (\text{with } H_{\ell+1} < H_\ell).$$

The theory predicts

$$||| \Pi_h u - u_h ||| = \mathcal{O}(h^k), \quad \|u - u_h^*\|_{L^2(\Omega)} = \mathcal{O}(h^{k+1}).$$

We confirm these rates for  $k = 1$  ( $P_1$  element) and  $k = 2$  ( $P_2$  element).

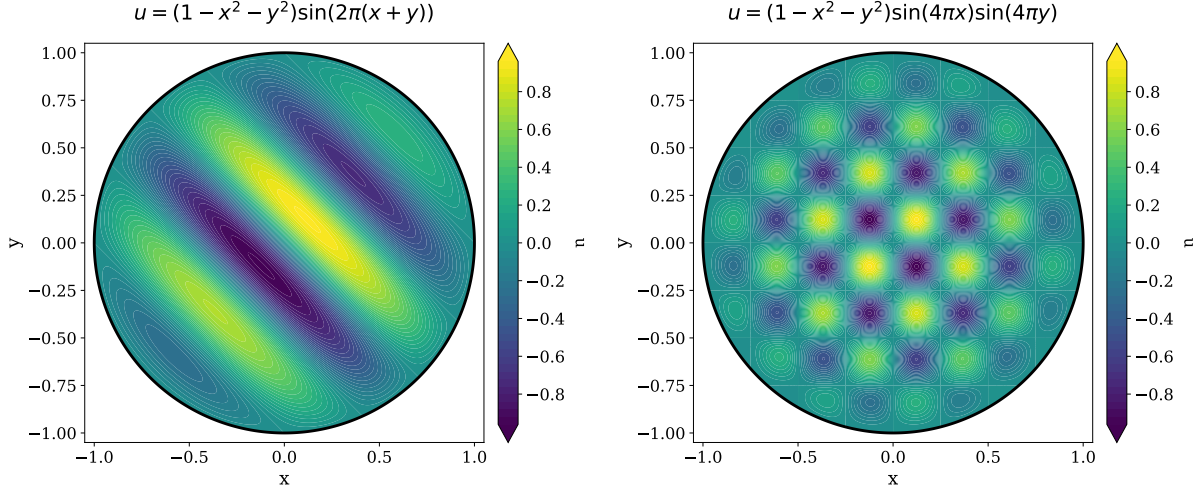


Figure 3: **Left:** graph of the exact solution for Test 1. **Right:** graph of the exact solution for Test 2. In comparison with Test 1, the solution for Test 2 exhibits higher oscillatory behavior.

### 5.1 Test 1: smooth manufactured solution on the unit disk

We choose the exact solution

$$u(x, y) = (1 - x^2 - y^2) \sin(2\pi(x + y)), \quad u|_{\partial\Omega} = 0,$$

with  $f = -\Delta u$  computed analytically, see the graph of  $u$  in the left of Figure 3. Numerical results are given in Table 1 and Table 2.

Table 1: Test 1 – Convergence Rate for  $P_1$  Elements

$H$	$    \Pi_h u - u_h    $	rate	$\ u - u_h^*\ _{L^2(\Omega)}$	rate
1/10	6.8137e-01	-	6.5392e-02	-
1/20	2.5475e-01	1.42	1.6092e-02	2.02
1/40	9.6410e-02	1.40	3.8834e-03	2.05
1/80	3.5411e-02	1.45	9.4701e-04	2.04
1/160	1.2741e-02	1.47	2.3242e-04	2.03

### 5.2 Test 2: oscillatory manufactured solution

To further challenge the discretization, we consider

$$u(x, y) = (1 - x^2 - y^2) \sin(4\pi x) \sin(4\pi y), \quad u|_{\partial\Omega} = 0,$$

with  $f = -\Delta u$  computed analytically. This test contains stronger oscillatory, see the right in Figure 3. Numerical results are given in Table 3 and Table 4.

Table 2: Test 1 – Convergence Rate for  $P_2$  Elements

$H$	$\ \Pi_h u - u_h\ $	rate	$\ u - u_h^*\ _{L^2(\Omega)}$	rate
1/10	2.2602e-01	-	8.9614e-03	-
1/20	4.1040e-02	2.46	8.5524e-04	3.39
1/40	7.2545e-03	2.50	8.3467e-05	3.36
1/80	1.2939e-03	2.49	8.6709e-06	3.27
1/160	2.3504e-04	2.46	9.6004e-07	3.18

Table 3: Test 2 – Convergence Rate for  $P_1$  Elements

$H$	$\ \Pi_h u - u_h\ $	rate	$\ u - u_h^*\ _{L^2(\Omega)}$	rate
1/10	1.0826e+00	-	1.3547e-01	-
1/20	4.7025e-01	1.20	3.7598e-02	1.85
1/40	1.9260e-01	1.29	9.5820e-03	1.97
1/80	7.0569e-02	1.45	2.3803e-03	2.01
1/160	2.5129e-02	1.49	5.8988e-04	2.01

Table 4: Test 2 – Convergence Rate for  $P_2$  Elements

$H$	$\ \Pi_h u - u_h\ $	rate	$\ u - u_h^*\ _{L^2(\Omega)}$	rate
1/10	6.2742e-01	-	2.5734e-02	-
1/20	1.0211e-01	2.62	2.5141e-03	3.36
1/40	1.7490e-02	2.55	2.7360e-04	3.20
1/80	3.2549e-03	2.43	3.2231e-05	3.09
1/160	6.4737e-04	2.33	3.9131e-06	3.04

### 5.3 DoF reduction compared to a fully nonconforming method

A key motivation for the coupled scheme is to avoid nonconforming unknowns in the interior. Although static condensation via the Schur complement and polynomial reduction are available in the literature, all degrees of freedom are counted here for a fair comparison. For  $k = 1$  the coupled method introduces, per WG element, 3 interior coefficients for  $v_0$  and per radial edge 2 trace dofs for  $v_b$ , while the interface dofs are shared with CG. For  $k = 2$  the counts become 6 interior coefficients per WG element and 3 trace dofs per radial edge. For  $k = 3, 4$ , the dofs can also be calculated similarly. To compare the degrees of freedom for CG and the coupled CG-WG scheme, we only consider dofs of CG in the interior region, the results are given in Table 5. To quantify savings, we report the ratio of total number of degrees of freedom for the coupled CG-WG scheme over dofs of full WG discretization on the same mesh, which is shown in Table 6.

Table 5: Ratio  $\frac{\text{CG dofs}}{\text{WG-CG dofs}}$  for  $P_k$  Elements

$H$	CG Element	WG Element	$P_1$	$P_2$	$P_3$	$P_4$
1/10	514	62	48.25%	66.16%	73.50%	77.36%
1/20	2275	125	65.77%	80.61%	85.63%	88.07%
1/40	9563	251	79.64%	89.56%	92.51%	93.88%
1/80	39220	502	88.78%	94.59%	96.19%	96.91%
1/160	158851	1005	94.09%	97.24%	98.07%	98.45%

Table 6: Ratio  $\frac{\text{WG-CG dofs}}{\text{Full-WG dofs}}$  for  $P_k$  Elements

$H$	CG Element	WG Element	$P_1$	$P_2$	$P_3$	$P_4$
1/10	514	62	17.33%	27.27%	35.54%	42.26%
1/20	2275	125	12.68%	23.02%	31.71%	38.80%
1/40	9563	251	10.47%	21.00%	29.88%	37.15%
1/80	39220	502	9.39%	20.01%	28.99%	36.34%
1/160	158851	1005	8.86%	19.53%	28.56%	35.95%

## 5.4 Observation

Across all tests, the numerical results in Tables 1–4 confirm the theoretical convergence orders:  $\mathcal{O}(h^k)$  in the energy norm and  $\mathcal{O}(h^{k+1})$  in  $L^2(\Omega)$ . The convergence rate for energy norm seems a bit higher constantly, though not proved here, we believe it is consistent with previous results, see [26] for a super-convergence results of energy norm. Moreover, Table 5 shows a comparable dofs for CG and WG-CG methods when the mesh is fine enough. Table 6 highlights that restricting weak Galerkin unknowns to the boundary layer substantially reduces the total dofs relative to a fully nonconforming discretization, while maintaining optimal accuracy.

## Declarations

### Conflict of interest

The authors declare that they have no conflict of interest.

### Data availability

The data and code generated during the current study are available from the authors upon reasonable request.

## References

- [1] Paola F Antonietti et al. “Review of discontinuous Galerkin finite element methods for partial differential equations on complicated domains”. In: *Building bridges: connections and challenges in modern approaches to numerical partial differential equations*. Springer, 2016, pp. 281–310.
- [2] Silvia Bertoluzza, Ilaria Perugia, and Daniele Prada. “A p-robust polygonal discontinuous Galerkin method with minus one stabilization”. In: *Mathematical Models and Methods in Applied Sciences* 31.13 (2021), pp. 2695–2731.
- [3] Silvia Bertoluzza and Daniele Prada. “A polygonal discontinuous Galerkin method with minus one stabilization”. In: *ESAIM: Mathematical Modelling and Numerical Analysis* 55 (2021), S785–S810.
- [4] Susanne C Brenner and L Ridgway Scott. *The mathematical theory of finite element methods*. Springer, 2008.
- [5] Erik Burman et al. “Cut finite element methods”. In: *Acta Numerica* 34 (2025), pp. 1–121.

- [6] Andrea Cangiani, Emmanuil H Georgoulis, and Paul Houston. “hp-version discontinuous Galerkin methods on polygonal and polyhedral meshes”. In: *Mathematical Models and Methods in Applied Sciences* 24.10 (2014), pp. 2009–2041.
- [7] Andrea Cangiani et al. “hp-version discontinuous Galerkin methods for advection-diffusion-reaction problems on polytopic meshes”. In: *ESAIM: Mathematical Modelling and Numerical Analysis* 50.3 (2016), pp. 699–725.
- [8] Philippe G Ciarlet. *The finite element method for elliptic problems*. SIAM, 2002.
- [9] Bernardo Cockburn and Manuel Solano. “Solving convection-diffusion problems on curved domains by extensions from subdomains”. In: *Journal of Scientific Computing* 59.2 (2014), pp. 512–543.
- [10] L Beirão Da Veiga, Alessandro Russo, and Giuseppe Vacca. “The virtual element method with curved edges”. In: *ESAIM: Mathematical Modelling and Numerical Analysis* 53.2 (2019), pp. 375–404.
- [11] Clint Dawson and Jennifer Proft. “Coupling of continuous and discontinuous Galerkin methods for transport problems”. In: *Computer Methods in Applied Mechanics and Engineering* 191.29-30 (2002), pp. 3213–3231.
- [12] Qingguang Guan. “Weak Galerkin finite element method for Poisson’s equation on polytopal meshes with small edges or faces”. In: *Journal of Computational and Applied Mathematics* 368 (2020), p. 112584.
- [13] Qingguang Guan, Max Gunzburger, and Wenju Zhao. “Weak-Galerkin finite element methods for a second-order elliptic variational inequality”. In: *Computer Methods in Applied Mechanics and Engineering* 337 (2018), pp. 677–688.
- [14] Qingguang Guan, Gillian Queisser, and Wenju Zhao. “Weak Galerkin finite element method for second order problems on curvilinear polytopal meshes with Lipschitz continuous edges or faces”. In: *Computers & Mathematics with Applications* 148 (2023), pp. 282–292.
- [15] Ceren Gürkan, Martin Kronbichler, and Sonia Fernández-Méndez. “eXtended hybridizable discontinuous Galerkin for incompressible flow problems with unfitted meshes and interfaces”. In: *International Journal for Numerical Methods in Engineering* 117.7 (2019), pp. 756–777.
- [16] Cuiyu He, Shun Zhang, and Xu Zhang. “Error analysis of Petrov-Galerkin immersed finite element methods”. In: *Computer Methods in Applied Mechanics and Engineering* 404 (2023), p. 115744.
- [17] Robert M Kirby, Spencer J Sherwin, and Bernardo Cockburn. “To CG or to HDG: a comparative study”. In: *Journal of Scientific Computing* 51.1 (2012), pp. 183–212.
- [18] Marc Lenoir. “Optimal isoparametric finite elements and error estimates for domains involving curved boundaries”. In: *SIAM journal on numerical analysis* 23.3 (1986), pp. 562–580.
- [19] Lin Mu, Junping Wang, and Xiu Ye. “Weak Galerkin Finite Element Methods on Polytopal Meshes”. In: *International Journal of Numerical Analysis and Modeling* 12.1 (2015), pp. 31–53.
- [20] Hui Peng et al. “Weak Galerkin and continuous Galerkin coupled finite element methods for the Stokes-Darcy interface problem”. In: *Communications in Computational Physics* 28.3 (2020), pp. 1147–1175.
- [21] Frits de Prenter et al. “Stability and Conditioning of Immersed Finite Element Methods: Analysis and Remedies: F. de Prenter et al.” In: *Archives of Computational Methods in Engineering* 30.6 (2023), pp. 3617–3656.

- [22] Manuel Solano and Felipe Vargas. “A High Order HDG Method for Stokes Flow in Curved Domains: M. Solano, F. Vargas”. In: *Journal of Scientific Computing* 79.3 (2019), pp. 1505–1533.
- [23] L Beirão da Veiga et al. “Polynomial preserving virtual elements with curved edges”. In: *Mathematical Models and Methods in Applied Sciences* 30.08 (2020), pp. 1555–1590.
- [24] L Beirão da Veiga, David Mora, and Alberth Silgado. “ $C^1$  virtual element methods on polygonal meshes with curved edges”. In: *arXiv preprint arXiv:2408.17381* (2024).
- [25] Junping Wang and Xiu Ye. “A weak Galerkin mixed finite element method for second order elliptic problems”. In: *Mathematics of Computation* 83.289 (2014), pp. 2101–2126.
- [26] Ruishu Wang et al. “Supercloseness analysis and polynomial preserving recovery for a class of weak Galerkin methods”. In: *Numerical Methods for Partial Differential Equations* 34.1 (2018), pp. 317–335.
- [27] Miloš Zlámal. “Curved elements in the finite element method. I”. In: *SIAM Journal on Numerical Analysis* 10.1 (1973), pp. 229–240.